

Finite temperature effects on cosmological baryon diffusion and inhomogeneous big-bang nucleosynthesis

In-Saeng Suh ^{*} and G. J. Mathews [†]
*Department of Physics, University of Notre Dame,
 Notre Dame, IN 46556, USA*

(August 10, 2021)

We have studied finite temperature corrections to the baryon transport cross sections and diffusion coefficients. These corrections are based upon our recently computed renormalized electron mass and modified state density due to the background thermal bath in the early universe. It is found that the optimum nucleosynthesis yields computed using our diffusion coefficients shift to longer distance scales by a factor of about 3. We also find that the primordial ${}^4\text{He}$ abundance decreases by $\Delta Y_p \simeq 0.01$ while D and ${}^7\text{Li}$ increase. Effects of these results on constraints from primordial nucleosynthesis are discussed. In particular, we find that a large baryonic contribution to the closure density ($\Omega_b h_{50}^2 \lesssim 0.4$) may be allowed in inhomogeneous models corrected for finite temperature.

PACS number(s): 98.80.Cq, 95.30.Tg, 26.35.+c

I. INTRODUCTION

It is generally believed that a cosmological phase transition from quark-gluon plasma to hadronic matter would have occurred when the temperature of the universe was about $T \simeq 100 \sim 200$ MeV [1,2]. This quark-hadron phase transition involves a rich variety of physical phenomena, particularly if it is first order. One possible consequence of this phase transition (or other mechanism [3] is the formation of isothermal baryon density fluctuations [2,4,3,5]. In particular, Applegate and Hogan [4] suggested that, once formed, such fluctuations could lead to the segregation of neutrons and protons. Baryon density inhomogeneities which persist to $T \sim 0.1$ MeV could affect primordial big-bang nucleosynthesis (BBN) yields. The primordial abundances of light elements in such inhomogeneous big-bang nucleosynthesis (IBBN) models would be quite different from those of the standard homogeneous big-bang nucleosynthesis (HBBN) model.

In the IBBN model, neutrons can diffuse relatively easily through the primordial plasma. Applegate, Hogan and Scherrer (AHS) [5] have shown that the different diffusion lengths for neutrons and protons could lead to the formation of high-baryon-density proton-rich regions and low-baryon-density neutron-rich regions. Before the freeze-out from weak reaction equilibrium (at $T \approx 1$ MeV), there is no segregation between neutrons and protons because the baryons only diffuse efficiently during

the fraction of the time they spend as neutrons. After weak equilibrium freeze-out, however, protons and neutrons diffuse independently. Since protons and neutrons have different diffusion coefficients, the result can be a spatial segregation of these species.

In view of the importance of using the light-element yields from BBN to constrain both the baryon-to-photon ratio and various cosmological and particle-physics theories [6], such IBBN models must be examined seriously. It is therefore important to evaluate the diffusion coefficients of neutrons and protons as accurately as possible in order to quantify the degree to which the primordial abundances of the light elements can be modified in the IBBN model. In this regard, AHS have derived the baryon diffusion coefficients using a mobility formula and the Einstein relation between mobility and the diffusion coefficient. After that, Banerjee and Chitre [7] used relativistic kinetic theory to calculate the baryon diffusion coefficients in the lowest order Chapman-Enskog approximation.

In calculations of the baryon diffusion coefficients, it is necessary to know the baryon transport cross sections for scattering with the background primordial plasma [5]. However, in all previous works, the transport scattering cross sections were calculated in vacuum and the electron mass was neglected. Therefore, in the present work we take into account finite temperature effects in the calculation of baryon diffusion coefficients and explore their

effects on primordial nucleosynthesis.

Finite temperature effects on elementary processes are significant from the point of view of cosmology and astrophysics. The early universe is usually described as a hot gas of particles in nearly thermodynamic equilibrium. Finite temperature effects enter through the statistical distribution functions which renormalize the masses and wave functions. These renormalized masses and wave functions affect scattering processes and decay rates.

Several authors [9] have generalized the electron mass and wave-function renormalization to all temperatures and densities. As an application of finite temperature effects, Dicus et al. [10], and independently Cambier et al. [11], included the finite temperature effects on weak reaction rates in the calculation of standard big-bang nucleosynthesis. They obtained the corrected light-element abundances and found that the corrections are only of order of a few percent. In subsequent work, Saleem [12] included the effects of the electron mass shift at finite temperature on BBN, and Baier et al. [13] examined the finite temperature radiative corrections to the weak neutron-proton decay rates. More recently, Fornengo et al. [14] have considered the finite temperature effects on the neutrino decoupling temperature which is important in the evolution of the early universe.

In this paper we calculate the baryon diffusion coefficients at finite temperature and apply these new diffusion coefficients to an IBBN model. We investigate finite temperature effects on the yields of primordial D , ${}^3\text{He}$, ${}^4\text{He}$, and ${}^7\text{Li}$ in the IBBN model. In the calculation of light element yields, we use a multi-zone computer code [15] which couples the diffusion equation with a nuclear reaction network and the cosmic expansion.

The plan of the paper is as follows. In Section II, we discuss how to include finite temperature effects in the calculation. We briefly discuss the effective mass of an electron with special attention to the $T \lesssim 1$ MeV temperature range which is most relevant for the neutron, proton diffusion before and during BBN. We also evaluate finite temperature effects on the baryon transport cross section in the scattering of baryons from the background electron-positron plasma. In Sec. III we calculate the baryon diffusion length with new diffusion coefficients for neutrons and protons and compare these to those estimated in AHS. In Sec. IV we apply our results to IBBN. Finally, we summarize our results and discuss the effects of finite temperature on light-element constraints from BBN. We shall employ units in which $\hbar = k_B = c = 1$, except when specific units must be attached to a result.

II. FINITE TEMPERATURE EFFECTS ON BARYON TRANSPORT CROSS SECTIONS

In the early universe where the particles are propagating in a thermal bath, their dynamics and interactions are modified relative to those in vacuum. This

behavior is systematically described in the framework of finite-temperature quantum field theory [16]. Finite temperature affects conditions in the early universe in the following ways. First of all, the free spinors used in the derivation of the cross section must be replaced by free finite-temperature spinors $u_T(p)$ which describe freely propagating particles in the background thermal bath. Also, the propagators are modified even at the tree level. Since these break the Lorentz invariance, they are absorbed into the effective mass for the particles. This effect can be evaluated by calculating the self-energy of the particle in the thermal bath. At the same time, finite temperature modifies the cross section due to the change of propagators and spinors in the scattering amplitude and in the distribution functions $f(E)$.

Secondly, the density of final states used in the determination of the cross section is modified by the background thermal bath as follows:

$$\frac{d^3 p'}{(2\pi)^3 2E'} \longrightarrow \frac{d^3 p'}{(2\pi)^3 2E'} [1 - f_F(E')], \quad (1)$$

where $f_F(E')$ is the Fermi-Dirac distribution at temperature T for final energy E' . This takes into account the states already occupied by fermions in the thermal bath. However, note that since we are still interested in single particle scattering, we do not make a thermal average over initial states.

The dynamics of electrons in a thermal bath is modified by the electromagnetic interactions with background photons and electrons themselves. Therefore, the effect of the thermal bath on the propagation of an electron is expressed by calculating the electron self-energy in the presence of the ambient e^+ , e^- and γ 's [9]. The temperature corrected electron physical mass is then obtained by evaluating the renormalized propagator and then finding the zero of its inverse. Thereby, the temperature dependent physical mass of an electron is given as [9]

$$m_T^2 \equiv m^2 = E^2 - \vec{p}^2 \\ = m_0^2 + \frac{2}{3}\alpha\pi T^2 + \frac{4}{\pi}\alpha m_0^2 \mathcal{B}(x) + \frac{\alpha}{2\pi^2} m_0^2 \mathcal{J}_A(p), \quad (2)$$

where $m_0 = 0.511$ MeV is the electron rest mass in vacuum and $\alpha = e^2/\hbar c$ is the electron fine structure constant. The function $\mathcal{B}(x)$ with $x = T/m_0$, is defined as [9]

$$\mathcal{B}(x) \equiv \int_1^\infty ds \frac{\sqrt{s^2 - 1}}{e^{s/x} + 1}. \quad (3)$$

In Ref. [14] it was shown that the function $\mathcal{J}_A(p)$ in the fourth term in Eq. (2) is negligible for $T \sim 1$ MeV. We therefore neglect this term in our analysis.

Eq. (2) is valid for all temperature [12]. It gives the correct result $m_T = m_0$ at $T = 0$. Around $T \sim m_0$, however, the third term becomes important and has to be taken into account [for example, $\mathcal{B}(x = 1) \simeq 0.543$].

It also has been shown in [14,17] that the thermal corrections to the electron mass at $T \sim \text{MeV}$ are sizeable. At $T = 1 \text{ MeV}$ the electron mass increases by 4.1%; and at $T = 2 \text{ MeV}$ the correction is as large as 16% [14].

Now we investigate the transport cross section in electron-hadron scattering at finite temperature. Rosenbluth [18] first calculated the electron-hadron differential cross section under the assumptions that the electron is ultrarelativistic ($m \ll E$) in the rest frame of the incoming hadron. This treatment takes into account the internal structure and anomalous magnetic moment. Applegate, Hogan and Scherrer [5] used the Rosenbluth formula in the calculation of the neutron diffusion coefficient, D_{ne} , with the assumption that the electron energy is much less than neutron mass M . They obtained a constant transport cross section σ_t for the vacuum interaction between an electron and a neutron [5],

$$\sigma_t^{AHS} = 3\pi \left(\frac{\alpha\kappa_n}{M} \right)^2 \simeq 8 \times 10^{-31} \text{ cm}^2, \quad (4)$$

where $\kappa_n = -1.913$ is the anomalous magnetic moment of the neutron. However, at $T \sim 1 \text{ MeV}$, the dynamical properties of electrons and photons in this thermal bath would be changed. (But neutrons would not be affected by the background thermal bath since their mass is nearly 2000 times the mass of the electron.) We therefore have to take into account the effect of finite temperature on the interaction between electrons and hadrons.

Recently, we calculated the temperature-dependent baryon transport scattering cross sections at finite temperature in the early universe [17]. The transport cross section $\sigma_t(T)$ of the scattering process is defined by

$$\sigma_t(T) = \int d\bar{\sigma} (1 - \cos\theta'), \quad (5)$$

where θ' is the scattering angle and $d\bar{\sigma}$ is the differential cross section including the thermal phase space. In the rest frame of the incoming neutron, $k^\mu = (k^0, k^i)$, where $k^0 = \epsilon = M$, and $k^i = 0$, integrating Eq. (5) over scattering angle, we obtained the temperature-dependent transport cross for electron-neutron scattering

$$\sigma_{ne}(T) = \frac{1}{2\pi} \frac{m^2 M}{|\vec{p}|^2} \int_{E'_{min}}^{E'_{max}} dE' (1 - \beta(E')) |\bar{\mathcal{M}}|^2 \mathcal{S}(E', \epsilon'), \quad (6)$$

where m is the mass of electron, M is the mass of neutron, $|\vec{p}|^2 = E^2 - m^2$, and

$$\beta(E') = \frac{E'(M + E) - m^2 - ME}{|\vec{p}'||\vec{p}|}. \quad (7)$$

The statistical factor $\mathcal{S}(E', \epsilon')$ is

$$\mathcal{S}(E', \epsilon') = [1 - f(E')][1 - f(\epsilon')], \quad (8)$$

where $f(E)$ is the Fermi-Dirac distribution function. For a given initial electron energy E , the kinematical limits

on the final state energy of the electron, E'_{min} and E'_{max} , can be determined from the constraint $|\cos\theta'| \leq 1$. The squared spin-averaged scattering matrix element in Eq. (6) is

$$|\bar{\mathcal{M}}|^2 = 2\pi^2 \left(\frac{\alpha\kappa_n}{mM} \right)^2 \left(\frac{1}{2} - \frac{EE' + m^2}{M(E' - E)} \right). \quad (9)$$

For electron-proton scattering, the most important scattering mechanism is Coulomb scattering and the differential cross section is given by the Mott formula. With the assumption that the electron energy is much less than the proton mass, the Coulomb transport cross section is [19],

$$\sigma_{pe}(T) = 4\pi\alpha^2 \left(\frac{E}{E^2 - m^2} \right)^2 \Lambda(T)[1 - f(E)]. \quad (10)$$

Because Eq. (10) diverges at small angles, the usual approximation is to truncate the angular integration at an angle given by the ratio of the Debye shielding length $\lambda_D = (T/e^2 n_e)^{1/2}$ to the thermal wave length $\lambda_{th} = (2\pi/mT)^{1/2}$ [7,8]. This defines the Coulomb logarithm $\Lambda(T) = \ln(\lambda_D/\lambda_{th})$. With this we can evaluate numerically the transport cross sections for a given initial electron energy.

In the early universe, the number density and energy density of electrons is given by [6]

$$n_e(T) = g_e \int \frac{d^3p}{(2\pi)^3} f(E), \quad (11)$$

$$\rho_e(T) = g_e \int \frac{d^3p}{(2\pi)^3} E f(E), \quad (12)$$

where g_e is the electron degeneracy. For an electron in thermal equilibrium, the phase space occupancy $f(E)$ is given by the Fermi-Dirac distribution

$$f(E) = \frac{1}{e^{(E-\mu)/T} + 1}, \quad (13)$$

where μ is the electron chemical potential. But since the chemical potential μ is small in the early universe, $\mu/T \lesssim 10^{-9}$ [10], we can ignore it in the numerical computations of the average electron energy. For the case in which the temperature dependent electron mass can not be neglected, we can obtain the average electron energy $\langle E \rangle = \rho_e/n_e$ from Eqs. (11) and (12). Since this initial electron energy $\langle E \rangle$ can be a good approximation in both relativistic and nonrelativistic limit [17], we will use it as the initial electron energy in numerical calculations of the scattering cross section. Fig. 1 shows the baryon transport cross section as a function of $x = T/m_0$ for the initial electron energy $E = \langle E \rangle$. For $T \lesssim 1 \text{ MeV}$, the electron-neutron transport cross section is not constant but increases as temperature decreases [17].

The change of mass of the particle could modify its contribution to the energy density of the universe and

therefore the expansion rate, but in this paper we will not consider this effect. In addition, the modification of the electron mass also changes the relationship between the neutrino and photon temperatures. The neutrino temperature differs from the photon temperature because neutrinos decouple at a temperature $T_d \simeq 1$ MeV. Therefore, they do not share in the entropy release from electron-positron annihilations which occurs at $T \lesssim 0.5$ MeV. The modified relationship between the neutrino and photon temperature is given by [10]

$$T_\nu = T_\gamma \left[\frac{4}{11} \zeta(w) \right]^{1/3} \quad (14)$$

where the function $\zeta(w)$ with $w = m/T_\gamma$ is defined by the integral

$$\zeta(w) = 1 + \frac{45}{2\pi^4} \frac{1}{w^4} \int_1^\infty ds \frac{s\sqrt{s^2-1}[s+(s^2-1)/3s]}{e^{s/w}+1} \quad (15)$$

In Eq. (14), we have neglected the density and pressure corrections [20] which give a small correction to the primordial ${}^4\text{He}$ abundance.

III. COSMOLOGICAL BARYON DIFFUSION

Baryon density inhomogeneities affect primordial nucleosynthesis through neutron-proton segregation. This segregation is determined by the different neutron and proton diffusion lengths during the nucleosynthesis epoch [2,4,3,5]. At high temperatures the diffusion lengths of neutrons and protons are equal because these particles intertransmute rapidly through weak interactions. After weak decoupling (at $T \approx 1$ MeV) neutrons and protons are no longer in equilibrium with respect to weak interactions. As a result, they retain their identity so that diffusive segregation can take place. Neutrons are scattered by electrons and positrons (through the interaction of their magnetic moments) and by protons due to nuclear interactions. Protons, on the other hand, undergo Coulomb scattering with electrons and are also scattered by neutrons. Other minor scattering mechanisms, such as neutron-photon scattering, neutron-neutron scattering, etc., may be neglected [5].

AHS [5] calculated the diffusion coefficients using a mobility formula together with the Einstein relation between mobility and the diffusion coefficient. They used a constant electron-neutron scattering cross section [Eq. (4)] and included a relativistic Maxwellian distribution for background light particles. Banerjee and Chitre [7] calculated the diffusion coefficients in the lowest order Chapman-Enskog approximation within the framework of relativistic kinetic theory. They showed the equivalence between the expression for the diffusion coefficients given by the mobility formula and that derived from relativistic kinetic theory for a dilute neutron gas diffusing

through electrons at low temperature. Kurki-Suonio, et al. [21] applied the new diffusion coefficients to IBBN and showed that the abundance curve shifted towards slightly larger distance scales. In the same spirit it is also of interest to investigate the effects of finite temperature on the baryon diffusion coefficients.

In relativistic kinetic theory [8], the diffusion coefficient of particle $i = n, p$ (neutron, proton) moving through a gas of light particles $j = e$ (electron), is given by [7,8,21]

$$D_{ij} = \frac{3}{8} \sqrt{\frac{\pi}{2}} \frac{1}{n_j \sigma_{ij}(T)} \frac{z^{1/2} K_2(z)}{K_{5/2}(z)} (1 - x_i), \quad (16)$$

where $z = T/m$ and x_i is the fraction of particles i and can be neglected [21]. $\sigma_{ij}(T)$ is the transport cross section for the scattering of particles i by particle j at temperature T . The modified Bessel functions, K_2 and $K_{5/2}$, are given by

$$K_2(z) = \frac{1}{z} \int_1^\infty dk k \sqrt{k^2 - 1} e^{-k/z}, \quad (17)$$

and

$$K_{5/2}(z) = \sqrt{\frac{\pi}{2}} \frac{\sqrt{z}(1 + 3z + 3z^2)}{e^{1/z}}. \quad (18)$$

In Eq. (16), $n_j (j = e)$ is the total density of electrons and positrons. At high temperature, $m_0 \lesssim T$, the electron density is given by the Fermi-Dirac distribution from Eq. (11). However, when the temperature is low enough that the net electrons dominate over the thermal electron-positron pairs, nonrelativistic Maxwell-Boltzmann statistics can be used to obtain the electron density. Then, overall charge neutrality requires that the net electron density be equal to the total density of protons. With this requirement, we can replace the electron chemical potential with the baryon-to-photon ratio η in a nucleosynthesis calculation. Thus, we obtain [21]

$$n_e = \left[2 \left(\frac{m}{\pi} T \right)^3 e^{-2m/T} + (\eta X_p n_\gamma)^2 \right]^{1/2}, \quad (19)$$

where X_p is proton mass fraction and n_γ is the photon number density. Note that the relative difference between the nonrelativistic Maxwell-Boltzmann and Fermi-Dirac statistics is small in the temperature range of interest. Therefore, we can use Eq. (19) in the calculation of baryon diffusion coefficients.

The neutron-proton diffusion coefficient is given by [5,7]

$$D_{np} = \frac{3\sqrt{\pi}}{4} \sqrt{\frac{T}{M_p}} \frac{1}{n_p \sigma_{np}} (1 - x_n), \quad (20)$$

where M_p is the proton mass, n_p is the proton number density, and σ_{np} is the neutron-proton scattering cross section. For our numerical calculations, we take the scattering cross section for s-wave neutron-proton scattering

given in Ref. [5]. As is Kurki-Suonio et al. [21], we use Eq. (20) in the calculation of baryon diffusion coefficients even though it comes from the Chapman-Enskog diffusion coefficient for classical hard-sphere scattering.

Finally, the effective neutron diffusion coefficient D_n is given by

$$D_n^{-1} = D_{ne}^{-1} + D_{np}^{-1}, \quad (21)$$

and the effective proton diffusion coefficient D_p is

$$D_p^{-1} = D_{pe}^{-1} + D_{pn}^{-1}, \quad (22)$$

where D_{pn} is the coefficient for the scattering of protons from neutrons. This quantity is related to D_{np} by [15]

$$D_{pn} = \left(\frac{X_p}{X_n} \right) D_{np}, \quad (23)$$

where X_n and X_p are the local neutron and proton mass fractions, respectively. (Note that this corrects the typographical error in Eq. (5) of Ref. [15] in which X_n and X_p are reversed.) Eq. (23) corrects D_{np} for the fact that the roles of the neutrons and protons are interchanged in the scattering leading to proton diffusion.

From Eqs. (21) and (22), we can compute the comoving diffusion length of baryons in the early universe. Here we take the comoving diffusion length relation from Refs. [5,22] in order to compare with those of AHS. Fig. 2 shows the comoving neutron and proton diffusion lengths as a function of temperature, where we have normalized the scale factor $R(t)$ to $R = 1$ when the neutrino temperature T_ν is 1 MeV. Our results are compared with the results of AHS for the case of $\eta_8 = 0.1$ ($\eta_8 = 10^8 \eta \simeq 0.67 \Omega_b h_{50}^2$), where h_{50} is the Hubble constant in units of $H_0 = 50 \text{ km s}^{-1} \text{ Mpc}^{-1}$.

The comoving baryon diffusion length at finite temperature is shifted to longer length scales by about a factor of 3 compared to the AHS estimate except the neutron diffusion length near $T \simeq 0.1$ MeV. The reason that both AHS and our comoving neutron diffusion lengths are equal around 0.1 MeV is due to the fact that D_{ne}^{FT} (where the superscript FT means that it was calculated with finite temperature corrections) intersects D_{ne}^{AHS} around 0.1 MeV. From these results, we see that finite temperature effect on baryon diffusion gives results which are roughly equivalent to those obtained using a smaller value of η .

IV. APPLICATIONS TO INHOMOGENEOUS BIG-BANG NUCLEOSYNTHESIS

As primordial abundance measurements become more refined, it may indeed turn out that the standard BBN model is no longer capable of fitting all of the observed abundances [23]. Indeed, if one adopts the currently favored lower D/H abundance of [24] together with the low Y_p of [25], a discrepancy may always exist [26]. In

this context, it is worthwhile to consider alternative cosmological nucleosynthesis models. One of the most extensively investigated possibilities is that of an inhomogeneous baryon density distribution at the epoch of nucleosynthesis. Such studies were initially motivated by speculation [1,2,4] that a first order quark-hadron phase transition (at $T \simeq 100 \sim 200$ MeV) could produce baryon density inhomogeneities as baryon number was trapped within bubbles of shrinking quark-gluon plasma. Other mechanisms also exist [3] for the generation of baryon inhomogeneities.

The abundances of primordial nucleosynthesis could be affected by these QCD motivated baryon inhomogeneities. There have been a number of studies on this subject [2,27]. Most studies in which the coupling between the baryon diffusion and nucleosynthesis has been properly accounted for [3,27] have concluded that the upper limit on $\Omega_b h_{50}^2$ is virtually unchanged when compared to the upper limit on $\Omega_b h_{50}^2$ derived from standard HBBN, where the allowed range for $\Omega_b h_{50}^2$ in HBBN is $0.04 \lesssim \Omega_b h_{50}^2 \lesssim 0.08$ [28,30,31]. However, in [28] and [30] it was shown that there exists a region of the parameter space for inhomogeneous models in which a somewhat higher baryonic contribution to the closure density is possible than that allowed in standard HBBN models. They found that a baryonic contribution as high as $\Omega_b h_{50}^2 \leq 0.13(0.2)$ (nearly twice the HBBN upper limit) is possible for the spherical (and cylindrical)-shell fluctuation geometry.

The purpose of this paper is, therefore, to estimate finite temperature effects on the IBBN model with our new diffusion coefficients and to investigate constraints on $\Omega_b h_{50}^2$. The calculations are based upon the coupled diffusion and nucleosynthesis code of Mathews et al. [15] with an initially square-wave spherical inhomogeneity. Since our study is focused only on finite temperature effects (and to compare directly with results of [15,21]), we do not include other effects [28] such as ion diffusion, Compton drag, other fluctuation shape geometry, and finite temperature corrections in weak interactions [10] which will also change BBN yields.

In order to describe the IBBN a number of parameters are introduced. The initial fluctuation shape is taken as regions of different baryon density separated by a sharp boundary. The physical quantities which characterize the fluctuation are the ratio of baryon number density, R , the mean separation between nucleation sites, r , the relative volume fraction f_V occupied by the high-density zones, and the total baryonic contribution to the closure density Ω_b . This latter quantity we relate to the baryon-to-photon ratio η by assuming a present background temperature of 2.75 K and a Hubble constant h_{50} .

We have performed the calculations with a range of parameters, and compare those results with the primordial abundances. We choose $R = 10^6$ and $f_V^{1/3} = 0.25$ for the high density region. For all calculations, we use three neutrino species and the neutron half-life $\tau_n = 10.70$ min-

utes [15]. The variable parameters in the calculations are the average separation distance between fluctuations r and the total average baryon-to-photon ratio η .

Fig. 3 shows the thermal evolution of the neutron and proton diffusion coefficients during the nucleosynthesis epoch for the parameters, $R = 10^6$, $f_V^{1/3} = 0.25$ and for the case of $\Omega_b h_{50}^2 = 0.1$ for $r = 100$ m. At high temperature ($T \gtrsim 0.1$ MeV), both D_n^{FT} and D_p^{FT} are much larger than those of AHS.

We also note that in our calculations neutron diffusion coefficients and proton diffusion coefficients are nearly independent of $\Omega_b h_{50}^2$ because the diffusion coefficients are dominated by electron scattering. The spike in the proton diffusion coefficient of AHS indicates neutron back diffusion [29]. The absence of a spike in our calculations indicates that there is little neutron back diffusion when finite temperature effects are included. This is because of the smaller D_n at low temperature.

The resulting abundances as a function of the distance scale of the inhomogeneity are shown in Figs. 4 and 5. The results are somewhat different from those of previous works [15,21]. It is found that the optimum nucleosynthesis yields computed using our diffusion coefficients is shifted to longer distance scales by a factor of about 3. We also can see that the value of the ${}^4\text{He}$ abundance significantly decreases by $\Delta Y_p \simeq 0.01$. There is also an increase in the primordial D and ${}^7\text{Li}$ abundance.

In order to see the allowed region for values of $\Omega_b h_{50}^2$ and r , we adopt the following observational constraints on the ${}^4\text{He}$ mass fraction Y_p from Ref. [28]:

$$0.226 \leq Y_p \leq 0.247. \quad (24)$$

For the primordial deuterium abundance, we adopt the constraints including implications of the possible detection of a high deuterium abundance in Lyman- α absorption systems [32] as an upper value, $D/H = 1.9 \pm 0.4 \times 10^{-4}$. The average lower value of D/H [24] is given as $D/H = 2.4 \pm 0.9 \times 10^{-5}$. Finally, we take a conservative upper limit on the primordial lithium abundance of ${}^7\text{Li}/H \leq 1.5 \times 10^{-9}$ [28] as well as the upper limit to the lithium abundance suggested in the detection (along with the possible depletion) of lithium in stellar atmospheres, ${}^7\text{Li}/H \leq 3.5 \times 10^{-10}$ [31].

Fig. 6 illustrates the allowed parameter region in the $\Omega_b h_{50}^2$ versus r plane for condensed sphere fluctuations for the adopted light-element abundance constraints. We note that, for the preferred low D/H abundance, no agreement is possible in the HBBN model without expanding both Y_p and Li limits. However, in the IBBN model a concordance region is possible between D/H and Y_p with the larger Li/H abundance upper limit.

We can see that the primordial lithium abundance crucially constrains the allowed values of $\Omega_b h_{50}^2$. This is because the back diffusion of neutrons which can destroy lithium [29] is hindered by the new diffusion coefficients. Nevertheless, by adopting a conservative upper limit to Li/H , large values of $\Omega_b h_{50}^2$ are allowed. The optimum

fluctuation distance scales ($20 \sim 60$ m) are about a factor of 3 larger than those implied by calculations using the AHS diffusion coefficients. With the larger value for the D constraint [32], allowed values of $\Omega_b h_{50}^2$ are nearly unchanged when compared to previous works [15,28,30]. However, for the smaller value of the D constraint [24] (together with a high lithium constraint), we obtain allowed values of $\Omega_b h_{50}^2$ as large as $\lesssim 0.4$!

V. CONCLUSIONS

We have studied the leading finite-temperature effects on baryon diffusion and nucleosynthesis in the early universe. The major motivation has been to quantify the degree to which finite-temperature effects could affect the nucleosynthesis constraints. We have calculated the baryon diffusion lengths based upon our previously calculated scattering cross sections [17] which included: (1) finite temperature Dirac spinors which are recast into the form of an effective electron mass; (2) finite temperature modifications to the phase space distribution of the electrons; and (3) the modified neutrino temperature.

The baryon diffusion coefficients which affect baryon inhomogeneities before or during big-bang nucleosynthesis are changed significantly by our temperature dependent electron-hadron transport cross sections. We have reevaluated the upper limits to $\Omega_b h_{50}^2$ in inhomogeneous primordial nucleosynthesis models which take into account finite temperature effects. The optimum conditions are shifted to larger fluctuation distance scales by a factor of about 3 in condensed spherical fluctuation geometry. It also is found that the value of ${}^4\text{He}$ decreases by $\Delta Y_p \simeq 0.01$. The limits on the baryon to photon ratio are constrained, however, by increased ${}^7\text{Li}$ which limits the allowed range of $\Omega_b h_{50}^2$.

With the larger value of the D constraints, allowed values of $\Omega_b h_{50}^2$ are nearly unchanged when compared to previous works. However, for the preferred smaller value of the D constraints, it is possible to have an allowed region of $\Omega_b h_{50}^2$ as large as 0.12 to 0.4 in inhomogeneous models.

Acknowledgments. The author would like to thank Prof. M. Orito for his careful reading of an early version of this manuscript. I.S.S. also acknowledges the Korea Research Foundation (KRF) for financial support. This work supported in part by DOE Nuclear Theory Grant DE-FG02-95ER40934.

[1] E. Witten, Phys. Rev. D **30**, 272 (1984).

- [2] K. Kajantie and H. Kurki-Suonio, Phys. Rev. D **34**, 1719 (1986); G. M. Fuller, G. J. Mathews and C. Alcock, *ibid* **37**, 1380 (1988); H. Reeves, Phys. Rep. **201**, 335 (1991); S. A. Bonometto and O. Pantano, *ibid.* **228**, 175 (1993) and references therein.
- [3] R. A. Malaney and G. J. Mathews, Phys. Rep. **229**, 145 (1993) and references therein; H. Kurki-Suonio and R. A. Matzner, Phys. Rev. D **37**, 2104 (1988); *ibid* **39**, 1046 (1990); *ibid* **42**, 1047 (1990); L. Rezzolla, *ibid* **54**, 6072 (1996).
- [4] J. H. Applegate and C. J. Hogan, Phys. Rev. D **31** 3037 (1985).
- [5] J. H. Applegate, C. J. Hogan and R. J. Scherrer, Phys. Rev. D **35** 1151 (1987).
- [6] E. W. Kolb and M. S. Turner, *The Early Universe* (Addison-Wesley, 1990).
- [7] B. Banerjee and S. M. Chitre, Phys. Lett. B **258**, 247 (1991).
- [8] S. R. de Groot, W. A. van Leeuwen and Ch. G. van Weert, *Relativistic kinetic theory* (North-Holland, Amsterdam, 1980).
- [9] J. F. Donoghue and B.R. Holstein, Phys. Rev. D **28**, 340 (1983); H. A. Weldon, *ibid* **26**, 1394 (1982); K. Ahmed and S. Saleem, *ibid* **35**, 1861 (1987); T. Toimela, Nucl. Phys. B**273**, 719 (1986).
- [10] D. A. Dicus *et al.*, Phys. Rev. D **26**, 2694 (1982).
- [11] J. L. Cambier, J. R. Primack and M. Sher, Nucl. Phys. B**209**, 372 (1982).
- [12] S. Saleem, Phys. Rev. D **36**, 2602 (1987).
- [13] R. Baier, E. Pilon, B. Pire and D. Schiff, Nucl. Phys. B**336**, 157 (1990).
- [14] N. Fornengo, C. W. Kim, and J. Song, Phys. Rev. D **56**, 5123, (1997).
- [15] G. J. Mathews, B. S. Meyer, C. Alcock, and G. M. Fuller, Astrophys. J. **358**, 36 (1990).
- [16] C. Bernard, Phys. Rev. D **9**, 3312 (1974); L. Dolan and R. Jackiw, *ibid* **9**, 3320 (1974); S. Weinberg, *ibid* **9**, 3357 (1974).
- [17] In-Saeng Suh and G. J. Mathews, astro-ph/9804090 Phys. Rev. D **58** in press.
- [18] M. N. Rosenbluth, Phys. Rev. **79**, 615 (1950).
- [19] W. Greiner and J. Reihardt, *Quantum Electrodynamics* (Springer-Verlag, Berlin, 1992).
- [20] A. F. Heckler, Phys. Rev. D **49**, 611 (1994).
- [21] H. Kurki-Suonio, M. B. Aufderheide, F. Graziani, G. J. Mathews, B. Banerjee, S. M. Chitre, and D. N. Schramm Phys. Lett. B **289**, 211 (1992)
- [22] J. H. Applegate, Phys. Rept. **163**, 141 (1988); N. Terasawa and K. Sato, Phys. Rev. D **39**, 2893 (1989); Prog. Theor. Phys. **81**, 254 (1989); *ibid* **81**, 1085 (1989)
- [23] G. J. Mathews, In-Saeng Suh, and T. Kajino, M. Orito, in *Particle Cosmology*, ed. K. Sato, T. Yanagida, and T. Shiromizu, (Universal Academy Press, Inc., Tokyo, Japan, 1998); C. Alcock, G. M. Fuller and G. J. Mathews, Astrophys. J. **320**, 439 (1987).
- [24] D. Tytler, X. M. Fan, and S. Burles, Nature, **381**, 207 (1996); S. Burles and D. Tytler, Astrophys. J. **460**, 584 (1996).
- [25] K. A. Olive, E. Skillman, and G. Steigman, astro-ph/9611166 (unpublished).
- [26] N. Hata, R. J. Scherrer, G. Steigman, D. Thomas, T. P. Walker, S. Bludman, and P. Langacker, Phys. Rev. Lett. **75**, 3977 (1995).
- [27] C. Alcock, G. M. Fuller and G. J. Mathews, Astrophys. J. **320**, 439 (1987); G. J. Mathews, D. N. Schramm, and B. S. Meyer, *ibid* **404**, 476 (1993); K. Jedamzik, G. M. Fuller, G. J. Mathews, and T. Kajino, *ibid* **422**, 423 (1994); K. Jedamzik, G. J. Mathews, and G. M. Fuller, *ibid* **423**, 50 (1994); *ibid* **441**, 465 (1995).
- [28] M. Orito, T. Kajino, R. N. Boyd, and G. J. Mathews, Astrophys. J. **488**, 515 (1997).
- [29] R. A. Malaney and W. A. Fowler Astrophys. J. Lett. **345**, L5 (1989).
- [30] G. J. Mathews, T. Kajino, and M. Orito Astrophys. J. **456**, 98 (1996).
- [31] C. J. Copi, D. N. Schramm, and M. S. Turner, Science., **267**, 192 (1995); Astrophys. J. **455**, L95 (1995).
- [32] A. Songaila, L. L. Cowie, C. J. Hogan, and M. Rugers, Nature, **368**, 599 (1994).

FIGURE CAPTIONS

Fig. 1 The baryon transport cross section as a function of $x = T/m_0$ for the initial electron energy $E = \langle E \rangle$. The solid line shows the temperature-dependent electron-neutron transport cross section. The dashed line denotes the electron-proton transport cross section.

Fig. 2 Comoving neutron and proton diffusion lengths as a function of temperature. Here we normalize the scale factor $R(t)$ to $R = 1$ when the neutrino temperature T_ν is 1 MeV. The solid line corresponds to the result of AHS. The dashed line is the comoving baryon diffusion length which takes into account finite temperature effects.

Fig. 3 The thermal evolution of the neutron and proton diffusion coefficients during the nucleosynthesis epoch for the fixed parameters, $R = 10^6$, $f_V^{1/3} = 0.25$, $r = 100 m$, and for the case $\Omega_b h_{50}^2 = 0.1$. The solid lines are results obtained using the AHS diffusion coefficients, the dashed lines are obtained with finite temperature corrections included.

Fig. 4 Light-element abundances as a function of the fluctuation distance scale for $\Omega_b h_{50}^2 = 1.0$. The initial baryon density ratio is $R = 10^6$ and the high density volume fraction is $f_V^{1/3} = 0.25$. The solid lines are results obtained using the AHS diffusion coefficients, the dashed lines are obtained with the diffusion coefficients in which finite temperature corrections are included. The fluctuation length scale r is given in units of meters comoving at $T = 100$ MeV. This calculation is based upon baryon density fluctuations represented by condensed spheres.

Fig. 5 Same as Fig. 4, but for $\Omega_b h_{50}^2 = 0.1$

Fig. 6 Allowed values for $\Omega_b h_{50}^2$ and the fluctuation length scale r based upon the various light-element abundance constraints as indicated. The fluctuation length scale r is given in units of meters comoving at $T = 100$ MeV. This calculation is based upon baryon density fluctuations represented by condensed spheres. The adopted primordial light-element abundance constraints are Y_p -1) $Y_p \leq 0.247$, Y_p -2) $Y_p \geq 0.226$; D-1) $D/H \geq 1.5 \times 10^{-5}$, D-2) $D/H \leq 3.3 \times 10^{-5}$, D-3) $D/H \geq 1.5 \times 10^{-4}$, D-4) $D/H \leq 2.3 \times 10^{-4}$; Li-1) ${}^7\text{Li}/H \leq 1.5 \times 10^{-9}$, Li-2) ${}^7\text{Li}/H \leq 3.5 \times 10^{-10}$. The single hatched region corresponds to the region allowed by the larger D constraints(D-3,D-4). The cross hatched region denotes the allowed region by smaller value of D constraints(D-1,D-2) plus the larger Li/H upper limit (Li-1).

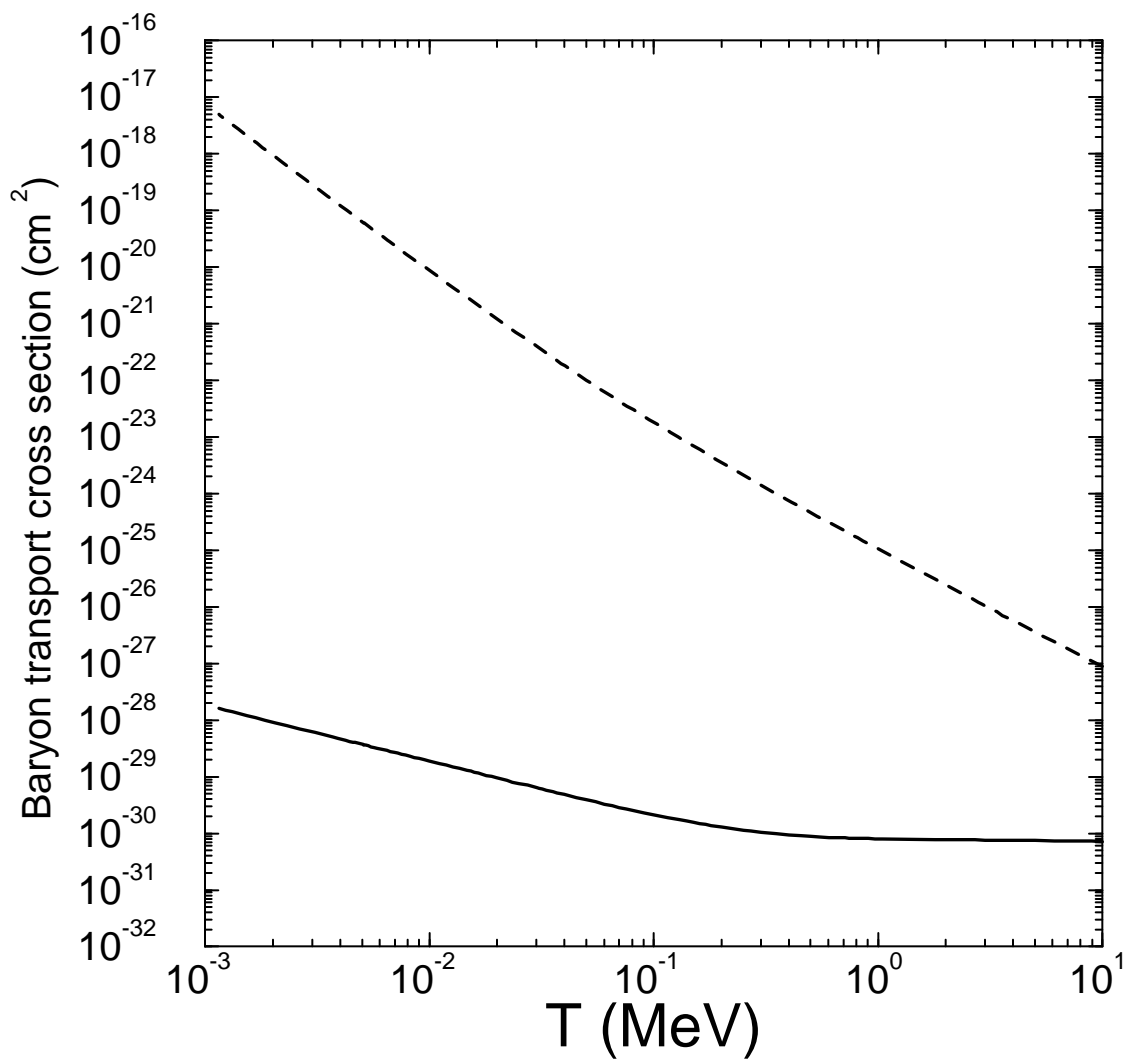


Fig. 1

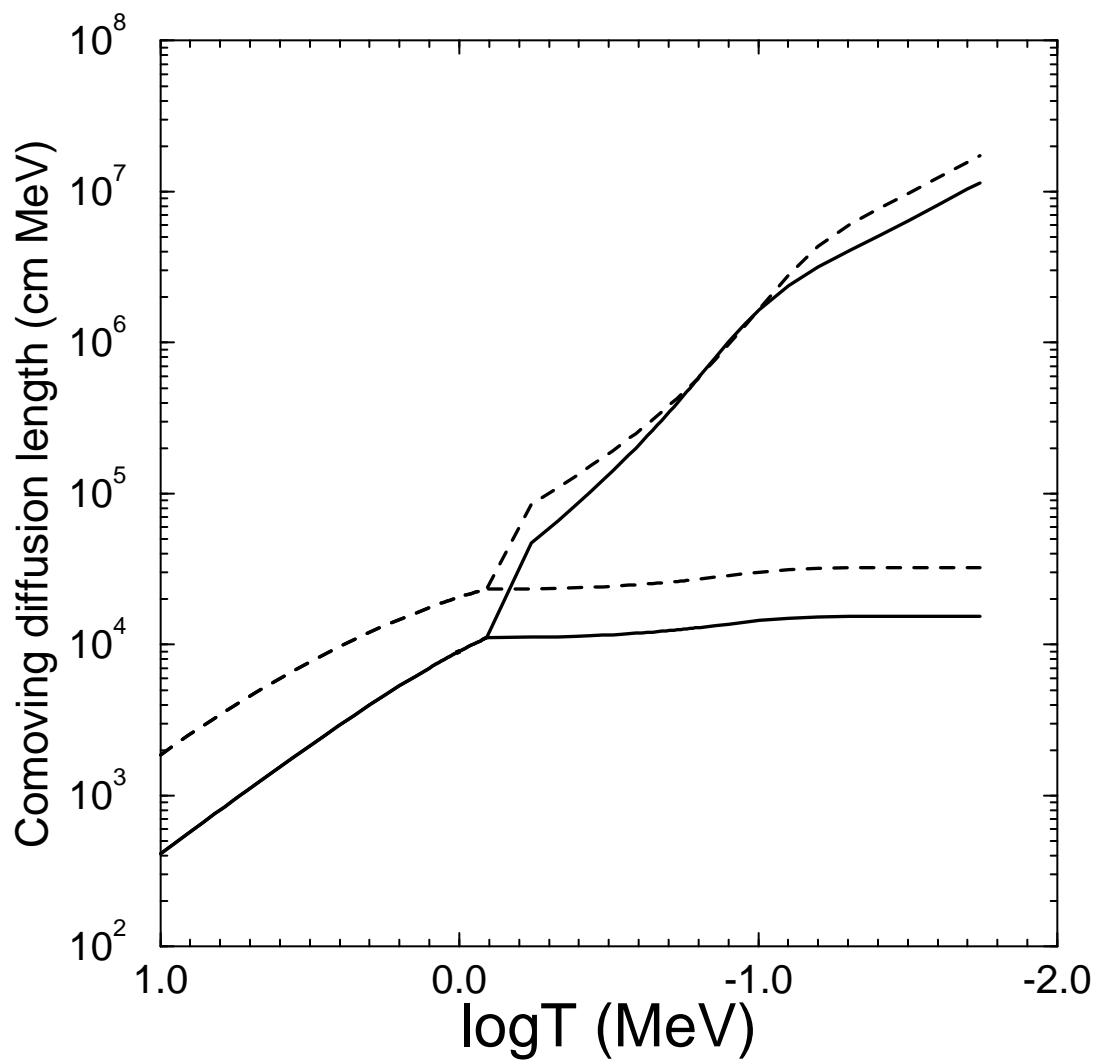


Fig. 2

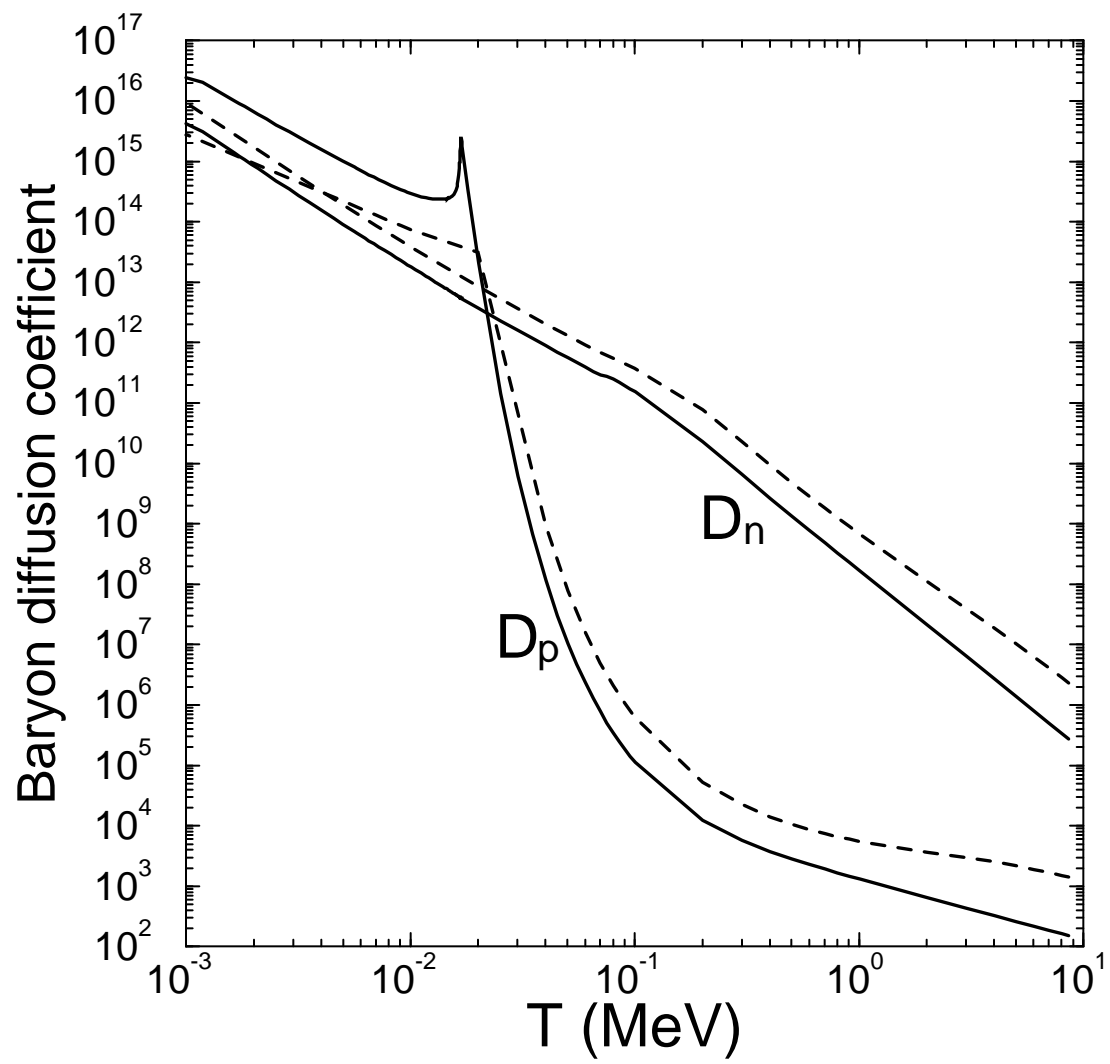


Fig. 3

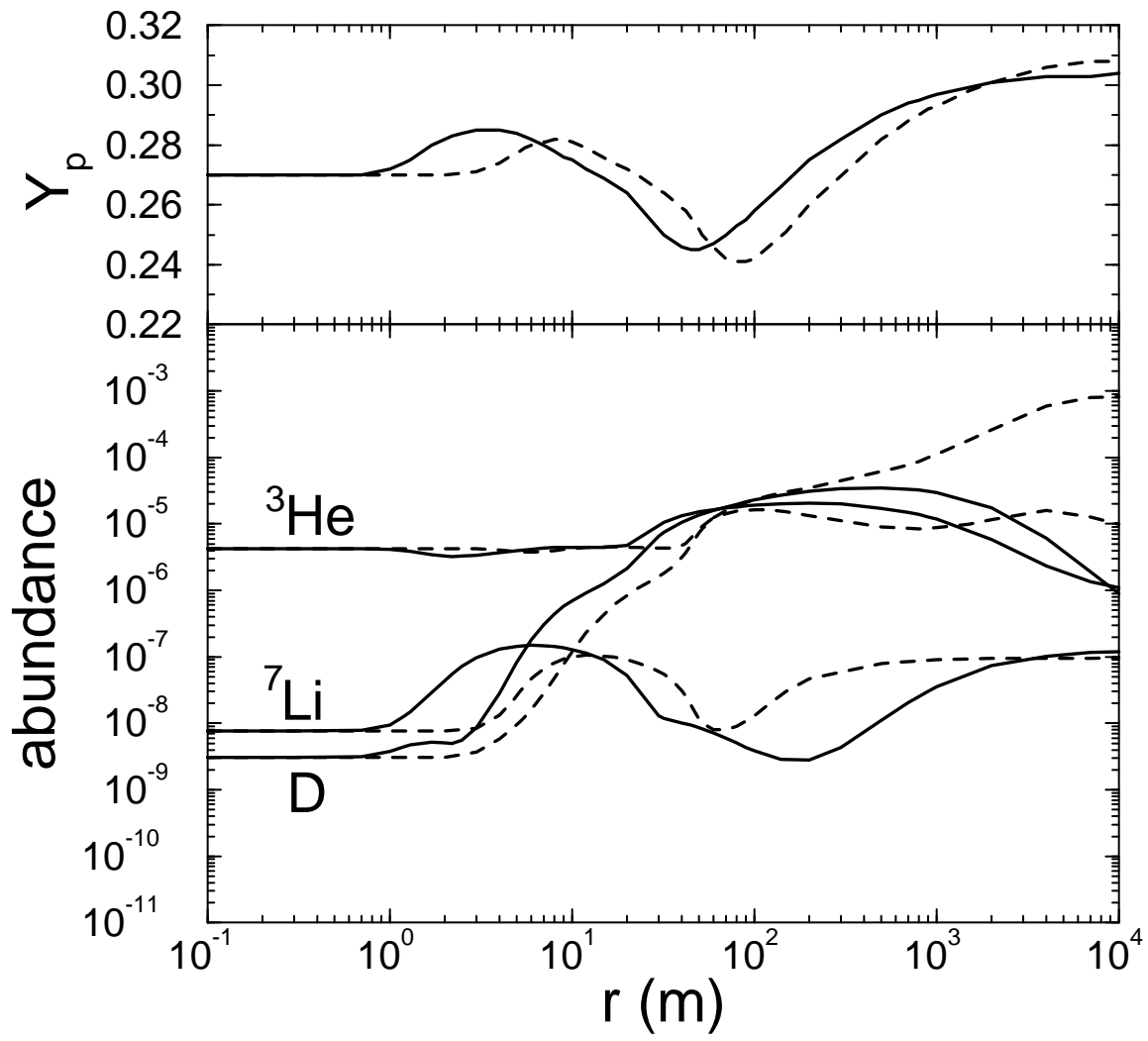


Fig. 4

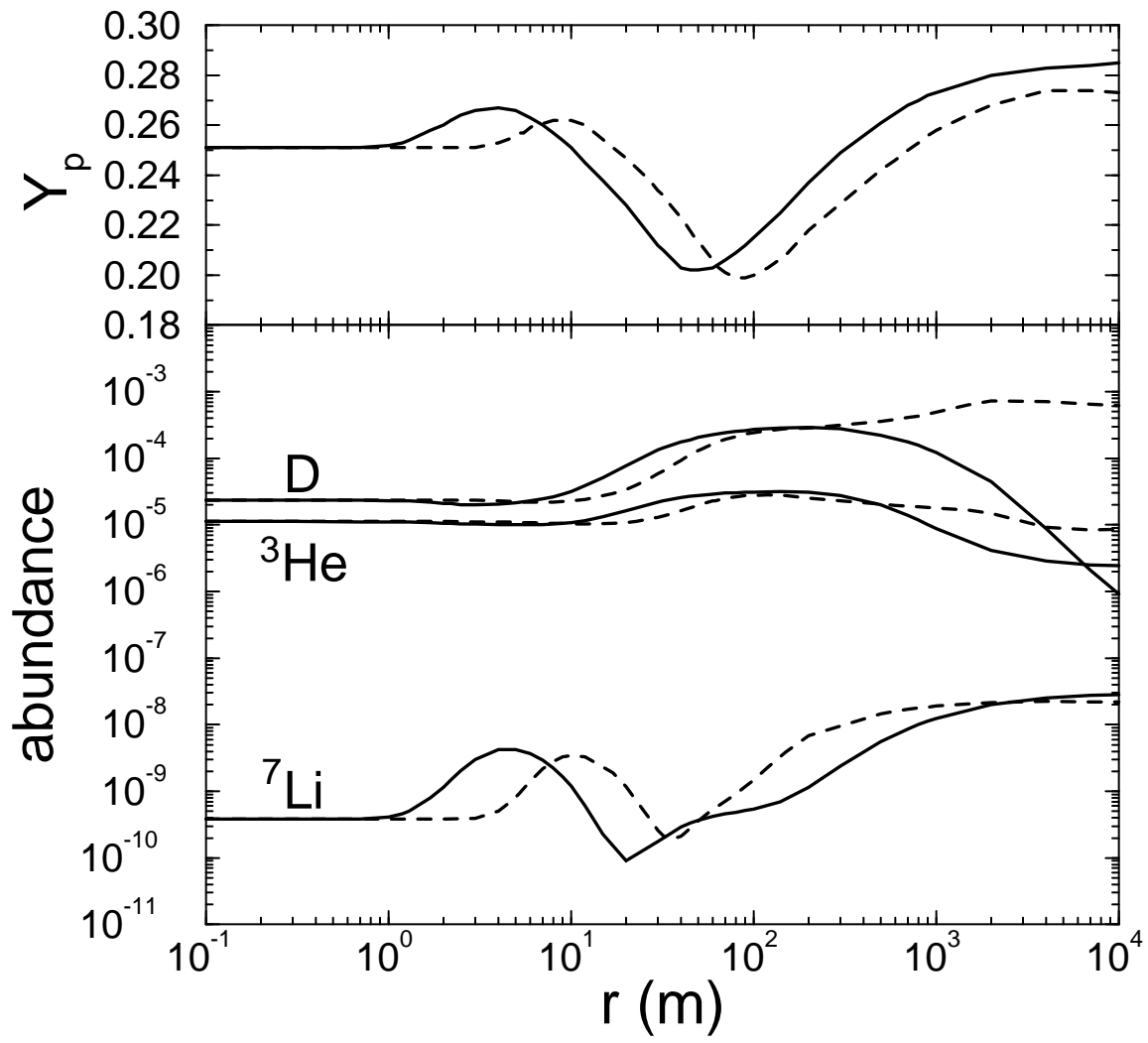


Fig. 5

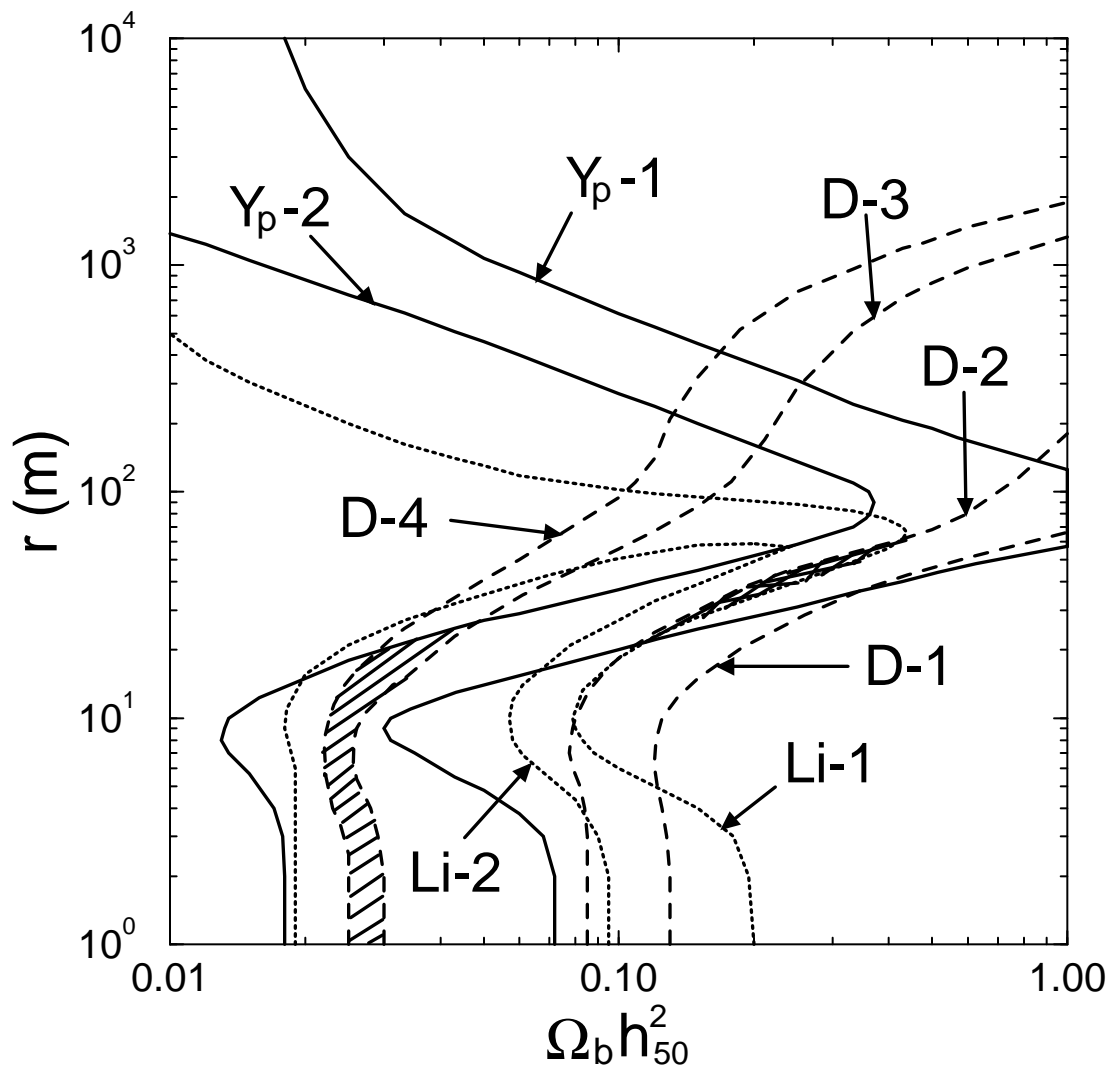


Fig. 6